# Causes of Long-Term Drought in the United States Great Plains

Siegfried D. Schubert, Max J. Suarez, Philip J. Pegion[1], and Randal Koster

Earth Sciences Directorate, NASA/GSFC

Greenbelt, Maryland

July 3, 2002

To be submitted to J. Climate

[1] Addition affiliation: Science Applications International Corporation, Beltsville, Maryland

## Abstract

The United States Great Plains (USGP) experienced a number of multi-year droughts during the last century, most notably the droughts of the 1930s and 1950s. This study examines the causes of such droughts using ensembles of long term (1930-1999) simulations carried out with the NASA Seasonal-to-Interannual Prediction Project (NSIPP-1) atmospheric general circulation model (AGCM) forced with observed sea surface temperatures (SSTs). The results show that the model produces long-term (multi-year) variations in the USGP precipitation that are similar to those observed.

A correlative analysis suggests that the ensemble mean low frequency (time scales longer than about 6 years) rainfall variations in the USGP are linked to a pan-Pacific pattern of SST variability that is the leading empirical orthogonal function (EOF) in the low frequency SST data. The link between the SST and the Great Plains precipitation is confirmed in idealized AGCM simulations, in which the model is forced by the 2 polarities of the pan-Pacific SST pattern. The idealized simulations further show that it is primarily the tropical part of the SST anomalies that influence the USGP. As such, the USGP tend to have above normal precipitation when the tropical Pacific SSTs are above normal, while there is a tendency for drought when the tropical SSTs are cold. The upper tropospheric response to the pan-Pacific SST EOF shows a global-scale pattern with a strong wave response in the Pacific and a substantial zonally-symmetric component in which USGP pluvial (drought) conditions are associated with reduced (enhanced) heights throughout the extra-tropics.

The potential predictability of rainfall in the USGP associated with SSTs is rather modest, with on average about 1/3 of the total low frequency rainfall variance forced by SST anomalies. Further idealized experiments with climatological SST, suggest that the remaining low frequency variance in the USGP precipitation is the result of interactions with soil moisture. In particular, simulations with soil moisture feedback show a six-fold increase in the variance in annual USGP

precipitation compared with simulations in which the soil feedback is excluded. In addition to increasing variance, the interactions with the soil introduce year-to-year memory in the hydrological cycle that is consistent with a red noise process, in which the low frequencies in the deep soil are the result of integrating a net forcing (precipitation – evaporation – runoff) that is white noise on interannual time scales. As such, the role of low frequency SST variability is to introduce a bias to the net forcing on the soil moisture that drives the random process preferentially to either wet or dry conditions.

## 1. Introduction

The USGP experienced a number of major droughts during the last century. The 1930s and 1950s droughts were the most extensive and long lasting. The 1930's drought affected about 2/3 of the country and parts of Canada, though the hardest impacted regions were the central and upper Great Plains (Felch 1978). It was during the 1930s drought that the southern Great Plains, including parts of New Mexico, Texas, Oklahoma, Colorado, and Kansas, was first characterized as the "Dust Bowl" (Worster 1979) - a reputation it earned from the numerous dust storms that occurred in that region during 1935-37 (Hughes 1976). The 1950's drought was most severe in the southern and central Great Plains. In Texas, it was the worst drought on record, with most of Texas not having what old timers called "a public rain" for 5 or 6 years (Hughes 1976). Dust storms were, however, less common than in the 1930s, apparently as a result of weaker winds during this time period (Borchert 1971).

Drought in the USGP is not unique to the last century. A number of proxy climate records indicate that multi-year droughts comparable to those of the 1930s and 1950s are, in fact, a regular feature of the Great Plains climate, having occurred approximately once or twice a century over the last 400 years (Woodhouse and Overpeck 1998). Looking still further back in time, there is evidence for multi-decadal droughts during the late thirteenth and sixteenth centuries that were of much greater severity and duration than those of the 20$^{th}$ century (Woodhouse and Overpeck 1998). For example, tree ring analyses in Nebraska suggest that the drought that began in 1276 lasted 38 years (Bark, 1978)!

Considerable research has been done on drought in the USGP. Examples include the studies by Namias (1955, 1982), Chang and Wallace (1987), Trenberth et al. (1988), Trenberth and Branstator (1992), Atlas et al. (1993), Lyon and Dole (995), Beljaars et al. (1996), and Mo et al. (1997). These and other studies have highlighted a number of potentially important factors contributing to dry conditions in the USGP, including extratropical and tropical Pacific SST anomalies, soil moisture, changes in the storm tracks, links with the adjacent Pacific and Atlantic anticyclones, and

changes in the Great Plains low level jet. The recent work by Koster et al. 2000 underscores the unique aspects of the Great Plains region that makes it particularly sensitive to changes in soil moisture.

While the above studies have contributed to our understanding of the processes that contribute to drought conditions in the USGPs, the mechanisms by which a drought can be maintained over many years have not yet been well established. The extent to which the SST anomalies contributing to drought are tied to the El Nino/Southern Oscillation (ENSO, e.g. Ropelewski and Halpert 1986) would appear to provide one mechanism for multi-year droughts, though the link with ENSO appears to be rather tenuous (except during some major events, e.g., Trenberth et al. 1988), and would not directly account for decadal long droughts such as the one that occurred during the 1930s. In fact the 1930s were marked by a distinct lack of ENSO activity (see, for example, Figure 3 in this study).

Several studies have examined the nature of long-term drought in the USGP. Ting and Wang (1997) show evidence for co-variability between U.S. summer precipitation and SST anomalies in the North Pacific Ocean on decadal time scales. Livezey and Smith (1999) show evidence for decadal co-variability between U.S. surface temperature and a pan-Pacific SST pattern that encompasses the tropics and extratropics. Barlow et al. (2000) distinguish between three modes of SST variability that they related to long-term drought in the United States: an ENSO mode, a decadal pan-Pacific mode, and a North Pacific mode. For example, the 1950s (1952-56) drought in the USGPs they associated with the cold phase of both the pan-Pacific and the ENSO mode, while the 1962-66 drought in the northeastern U.S. they associated with the North Pacific mode.

In this paper, we present an analysis of long term USGP drought in an ensemble of nine 70-year (1930-1999) simulations carried out with the NSIPP-1 AGCM forced by observed sea surface temperatures. Our focus is on assessing the causes and predictability of the simulated droughts. Section 2 describes the model simulations and the observations. The results from the 70-year

simulations forced by observed SST are described in Section 3. Section 4 presents the results from some idealized SST experiments. Section 5 examines the role of land-atmosphere feedbacks. The discussion and conclusions are given in Section 6.

## 2. The AGCM simulations and observations

The simulations were carried out with the NASA Seasonal-to-Interannual Prediction Project (NSIPP-1) atmospheric-land general circulation model (AGCM). The model is part of the NSIPP coupled atmosphere-land-ocean model; however, for these experiments, it is run uncoupled from the ocean. The NSIPP-1 AGCM is a grid-point model. The dynamical core is described in Suarez and Takacs (1995). The boundary layer scheme is a simple K-scheme, which calculates turbulent diffusivities for heat and momentum based on Monin-Obukhov similarity theory (Louis et al., 1982). The AGCM uses the relaxed Arakawa-Schubert (RAS) scheme to parameterize convection (Moorthi and Suarez, 1992). The parameterization of solar and infrared radiative heating is described in Chou and Suarez (1994, 1999). The mosaic model (Koster and Suarez, 1996) is used to represent land processes. The simulations described here use a uniform horizontal resolution of 2° latitude by 2.5° longitude and 34 unequally spaced $\sigma$-layers with high resolution (<200 m) in the lower 2 km of the atmosphere. Details of the NSIPP-1 model formulation and its climate are described in Bacmeister et al. (2000). The seasonal predictability of the model is described in Pegion et al. (2000) for boreal winter, and in Schubert et al. (2001) for boreal summer.

The simulations consist of an ensemble of nine 70-year (1930-1999) runs forced by observed monthly sea surface temperatures. The runs differ only in their initial atmospheric conditions: these were chosen arbitrarily from previously completed simulations. Since this study was started before the availability of the newest long-term Hadley SST products (see below), we used SSTs constructed from three different monthly products. For the period 1930-48 these are an early version of the Hadley product (Rayner et al. 2002). For the period 1949-81 they are the

GISST product (Rayner et al. 1996), and for the period 1982-99 they are from Reynolds and Smith (1994). While we attempted to correct for bias in the three SST products, an analysis of our combined SST record nevertheless showed evidence of some discontinuities. To reduce the impact on our results of these discontinuities in the SST record we have removed from the 70-year simulations and related observations (as part of the post-processing steps) the three means (1930-48, 1949-81, 1982-99) separately. As a consequence, our results contain no information on any long-term trends that may exist in the data.

Another factor that potentially impacts the results is that each model simulation was not carried out as a single continuous run. The runs were instead produced in stages with the first set (seven of the nine ensemble members) of runs starting in December of 1978. The earlier periods were then back-filled, with the second set starting December 1960, and the third set starting in November of 1929. The eighth and ninth ensemble members were started in 1950, and then were back-filled starting in 1929. While these discontinuities should not impact our analysis of the ensemble mean, we are careful to note in the text where calculations (e.g. filters) involving the individual ensemble members might be impacted.

The model results are compared with the Global Historical Climatology Network (GHCN) station precipitation data (Vose et al. 1992), which are available for the period 1930-1981, and the combined station and satellite estimates of Xie and Arkin (1996), for the more recent period 1982-1999. The upper-air fields are compared with the NCEP/NCAR reanalysis (Kalnay et al. 1996) for the period 1950-99.

The boreal summer climatology of the NSIPP-1 model is presented in Bacmeister et al. (2000) and is not repeated here. The model does well in reproducing the global distribution of the JJA upper level height and velocity potential fields. In particular, it produces the climatological high over North America with about the correct amplitude and position. The model also does a reasonable job of reproducing the JJA observed global distribution of precipitation, though like many models, it

underestimates the precipitation in the eastern Pacific ITCZ, and overestimates the precipitation over the eastern United States. The model also tends to extend high precipitation amounts too far west over the central Great Plains.

## 3. Drought Signal Forced by SST

We begin by presenting in this section the results from the nine 70-year simulations forced by observed SST. The results (simulations and observations) have the three means removed as describe above, and are filtered using a low frequency filter (Zhang et al. 1997) that retains time scales of about 6 years and longer. The filter effectively removes ENSO variability allowing us to focus attention on the longer-scale fluctuations such as those that occurred during the 1950s and 1930s. In the following, we refer to this filter simply as the low frequency filter, and the filtered quantities as low frequency quantities.

The thin black curves in Figure 1 denote the low frequency precipitation from the nine ensemble members averaged over roughly the USGP region (30-50°N, 95-105°W). The curves are dashed for those time periods where the results are affected by the discontinuities in the simulations as described in section 2. The dashed lines span about 60 months (the length of the low frequency filter). The heavy solid curve is the low frequency ensemble mean. The heavy dashed curve is the observed low frequency rainfall. The results show considerable scatter among the ensemble members though there are clearly time periods during which the curves tend to follow one another. For example, during the 1930's almost all the runs show a tendency for dry conditions, consistent with the observations. This is followed, in the early 1940's, by wet conditions, again consistent with the observations. On the other hand, during the 1950's, the runs show a mixture of dry and wet conditions. Only one of the nine runs is as dry as what was observed. Most of the runs show dry conditions during the mid 1970s, while the observations show a tendency for wet or neutral conditions. During the last two decades almost all the ensemble members show pronounced fluctuations in rainfall that are generally consistent with the observations.

The above results suggest that the model behavior is not inconsistent with the observations in the sense that the observations fall within the spread of the ensemble members. Focusing on the model ensemble results, we see that there are times when the rainfall is potential predictability if the SSTs are known. In particular, the 1930s drought (with almost all ensemble members showing negative rainfall anomalies throughout much of the decade) appears to have been predictable, but the 1950s drought does not. On average, the contribution of the SST forced response to the total simulated low frequency precipitation variance is rather modest over the USGP. Table 1 shows the contributions of the signal (Rowell at al. 1995) and noise to the total variance in the USGP precipitation for various time scales. For the low frequencies (time scales longer than 6 years) the signal to noise ratio is 1/2 or, equivalently, the ratio of the ensemble mean variance to the total low frequency variance is 1/3. For comparison, the signal/noise ratio for the annual means is somewhat larger (0.56), while the seasonal means show

| | **Signal** | **Noise** | **Total** | **Signal/Noise** |
|---|---|---|---|---|
| **DJF** | .0052 | .0448 | .05 | .12 |
| **MAM** | .0184 | .0826 | .0101 | .22 |
| **JJA** | .0933 | .3382 | .4315 | .28 |
| **SON** | .0184 | .0826 | .1010 | .22 |
| **Annual Mean** | .0267 | .0479 | .0746 | .56 |
| **Low Frequency** | .0072 | .0146 | .0219 | .49 |

Table 1: The signal variance, the noise variance, the total variance, and the signal/noise ratio for the precipitation averaged over the USGP (30°-50°N, 95°-105°W). Units are in $(mm/day)^2$ except for the signal/noise which is dimensionless. Results are from the 9 model simulations for the period 1930-99. The different rows correspond to the four seasonal means, the annual mean, and the low pass filtered data (time scales longer than 6 years).

considerably smaller signal to noise ratios that range from 0.12 for boreal winter, to 0.28 for boreal summer. Note, however, that the amount of variance within the various time scales differs considerably. For example, the low frequencies account for only about 30% of the variance of the annual mean values.

The correlations between the low frequency ensemble-mean USGP precipitation and the SST (top panel of Figure 2) show large-scale coherence. A test based on a Fisher's Z-transform of the correlations (Stuart and Ord, 1994), and assuming 12 (25) degrees of freedom in the filtered time series indicates absolute values greater than 0.57 (0.39) are significantly different from zero at the 5% level. Wet conditions in the USGP are associated with warm SST anomalies throughout the central tropical Pacific and the North Pacific just off the west coast of North America, warm anomalies over much of the South Pacific, cold anomalies in a v-shape extending eastward and poleward into both hemispheres from the Pacific warm pool, and cold anomalies in the tropical Atlantic.

The SST correlation pattern in Fig. 2 is similar to that found in several previous observational studies. For example, Barlow et al. (2001) find a very similar SST pattern as the second leading mode of monthly Pacific SST variability during 1945-93. Zhang et al. (1997) and Mantua et al. (1997) also find comparable low-frequency SST patterns, though with larger anomalies in the eastern tropical Pacific. Repeating our SST correlation calculations using the observed low frequency USGP precipitation, shows an SST correlation pattern (not shown) that bears some similarity to that in Fig. 2. The correlations, however, tend to be weaker and in fact the strongest positive correlations are with the SST in the Indian Ocean and the southern middle/high latitude oceans, while the strongest negative correlations occur with SST in the North Atlantic. It is important to emphasize, however, that the SST correlation pattern in Fig. 2 is based on the ensemble mean precipitation, and individual ensemble members (including the observations) may produce different correlations. For example, for one of the ensemble members the correlations with SST are close to zero almost everywhere, for another, the correlations are predominantly positive throughout the Pacific and Atlantic Oceans, while for several others the correlations closely resemble the results for the ensemble mean (results

not shown). This serves to highlight the weakness of the link between the SST and the USGP precipitation (recall that the SST account for only about 1/3 of the variance), and the fact that individual ensemble members (including the observations) do not provide a good estimate of the relationship between the USGP precipitation and the SST.

We can obtain some idea of the spatial scale of the simulated USGP precipitation fluctuations by correlating the low frequency ensemble mean USGP precipitation with the low-frequency ensemble mean precipitation at all other grid points (Figure 2: middle panel). The correlations show that in the model, precipitation fluctuations in the USGP on long time scales tend to be coherent over much of the continental United States (especially the southern half of the U.S. and extending into Mexico). Furthermore, the fluctuations have coherence on a global scale, with a tendency for fluctuations of like sign occurring throughout the northern middle latitudes, the southern middle latitudes, and in a region extending from the central tropical Pacific towards southern South America. Fluctuations tend to be of opposite sign to those in the USGP in the South Pacific Convergence Zone (SPCZ), the high latitude southern oceans, southern Asia, and the tropical Atlantic. The bottom panel of Figure 2 shows the correlations of the low-frequency ensemble-mean USGP precipitation with the low-frequency ensemble mean 200mb height field. The USGP precipitation is associated with global scale height anomalies consisting of a strong wave response emanating from the tropical Pacific into both hemispheres, and a substantial zonally-symmetric component. Dry conditions are associated with positive height anomalies in the middle latitudes of both hemispheres, and reduced heights in the tropics and the high latitudes. In general, the height anomalies implied by the correlations appear to be consistent with the tropical precipitation anomalies suggested by the middle panel of Figure 2. For example, wet conditions off the west coast of the United States are associated with an enhanced trough over the North Pacific that would presumably produce more storm systems over the eastern North Pacific.

In order to better establish the link between the SST and the USGP precipitation, we first compute the EOFs (using varimax rotation) of the low frequency SST for the period 1932-1998. The upper

left panel of Fig. 3 shows that the leading EOF has a spatial structure that is very similar to the correlation pattern between the USGP and precipitation shown in Fig. 2. For comparison with our low frequency pattern (upper left panel of Fig. 3), we show in the upper right panel of Fig. 3 the leading EOF of the residual SST field (total SST – low frequency SST). This pattern is largely confined to the tropical central and eastern Pacific and is clearly related to ENSO (see also below).

The time series (principal components or PCs) corresponding to the above two leading SST EOFs are shown in the lower panel of Fig. 3. The low pass PC shows substantial negative values during the 1930s, 1950s and 1970s, indicating from the correlation analysis that those periods should be characterized by dry conditions in the USGP. The largest positive values occur in the early 1940s, the late 1950s and 1960s, and the early 1990s, indicating wet conditions should prevail in the USGP during these periods. The residual PC shows large positive values (warm Pacific SST) occurring during 1972/73, 1982/83, 1986/87 and 1997/98, consist with a strong link of this mode to ENSO. There is also a dramatic change in the character of the ENSO signal with much reduced ENSO activity prior to about 1960 (especially during the 1930s). We will discuss the potential implications of that change in ENSO for drought in the USGP in the last section.

We next correlate the leading low frequency SST PC shown in Fig. 3 with precipitation at all grid points (top panel of Fig. 4). The pattern is remarkably similar to that produced earlier (middle panel of Fig. 2) involving the correlation between the USGP precipitation and precipitation at all grid points. This serves to further highlight that the low frequency ensemble mean USGP precipitation is linked to a dominant global-scale mode of SST variability. For comparison, the lower panel of Fig. 4 shows the correlation between the leading residual (total monthly minus low frequency) SST PC (Fig. 3) with the ensemble mean residual precipitation. In these calculations, the residuals are based on monthly mean values and a 5-month running mean is applied before computing the correlations. Here, correlations with absolute value greater than 0.28 are significantly different from zero at the 5% level. The test is again based on a Fisher's Z-transform of the correlations, though we assume here about 50 degrees of freedom for the residual ensemble mean time series. Compared with the low

frequency results, the correlations for the residuals have somewhat smaller magnitudes, though the spatial patterns show substantial similarities. The largest differences are in the eastern tropical Pacific and over much of North America. In the eastern tropical Pacific, the residual shows a strong ENSO connection with positive correlations extending all the way to South America and negative anomalies to the north, while the low frequency results show little correlation in the eastern tropical Pacific. The maximum positive correlations in the tropical Pacific are in somewhat different locations, with the residual correlation maximum located just east of the dateline, and the low frequency correlation located just west of the dateline. There are also substantial differences over North America, with strong positive correlations over much of the continent for the low frequency results, and only weak correlations in the southern U.S., Mexico and along the west coast for the residual calculation.

## 4. Idealized SST

The above results suggest that low frequency variations in USGP precipitation are, at least in part, controlled by large-scale pan-Pacific SST anomalies that resemble the leading low frequency EOF shown in the top left panel of Fig. 3. We next describe a series of model simulations that are forced with idealized SST anomalies consisting of that leading low frequency EOF. For this purpose, we have recomputed the leading low frequency SST EOF from the more recent HadISST dataset (Rayner et al. 2002). We do this to circumvent the problem of trying to define an SST climatology from the three different SST data sets used in the 70-year model runs. The leading low frequency EOF computed from the HadISST data set (not shown) is generally quite similar to that shown in Figure 3, though it has somewhat more amplitude in the Indian Ocean and the far eastern tropical Pacific south of the equator, and less amplitude in the North Atlantic Ocean.

Three runs were carried out consisting of two 40-year simulations that were forced by the two polarities of the low frequency SST EOF (with an amplitude of two standard deviations), and a third 100-year run with climatological SSTs (a repeating seasonal cycle). The results for the 200mb height

field are shown in Figure 5. Here we compare the annual mean anomalies (Dec-Nov mean deviations from the climatological run) for the positive and negative phases of the idealized SST runs (bottom panels), with the analogous fields from the ensemble mean of the original nine 70 year runs. The latter are computed by compositing the height fields based on the amplitude of the low frequency SST EOF in the 70 year runs. Time periods when the SST EOF is greater than +1 standard deviation contribute to the positive composite, while time periods when the SST EOF is less than –1 standard deviation contribute to the negative composite (upper panels). The composite fields are then scaled to make them representative of a 2-standard-deviation anomaly. We take this approach (instead of compositing based on 2 standard deviations in the SST EOF) to obtain more realizations in the composites. We further change the sign of the negative anomalies (right panels) to help identify nonlinearities in the response to the pan Pacific SST EOF. Comparing the results for the positive phase and the positive composite (left panels of Figure 5) shows that the composite anomaly is quite well reproduced by forcing the model with only the low frequency EOF. There is also considerable similarity between the negative composite and the negative phase of the idealized run, though in this case there are substantial differences, especially over the North Pacific and North America. This difference appears to be the result of a substantial non-linearity in the response to the idealized SST. The negative (or cold) phase of the EOF forcing produces a generally weaker response in the extratropics compared with the positive (or warm) phase. Such a nonlinearity in the response is much less evident from the composites of the full SST forced runs (top panels of Figure 5). Any potential nonlinearity may, however, be masked in these results, since the averaging done to produce the climatology would, by definition, include the effect of the nonlinearity and therefore tend to make the positive and negative anomalies more symmetric.

Figure 6 is the same as Figure 5, except for precipitation. The precipitation also shows generally good agreement between the idealized run and the composite from the 70 year runs for the positive or warm phase. The left panels of Figure 6 both show large positive anomalies in the central tropical Pacific and negative anomalies to the west and to the south. Both also show a tendency for wet conditions over the USGP. The negative or cold phase also shows generally good agreement between

the idealized and full SST runs. Both fields show a tendency for dry conditions over the USGP. Here there is, surprisingly, less evidence for non-linearity than for the heights, though there is some tendency for weaker precipitation anomalies in the central tropical Pacific for the negative phase (compare bottom panels of Figure 6).

Figures 7 and 8 are the same as the bottom panels of Figures 5 and 6, respectively, except that we show separately the composite anomalies for each season. We have again changed the sign of the negative anomalies to help identify nonlinearities in the response to the pan Pacific SST EOF. The results show a clear seasonal evolution in both the precipitation and 200mb height response. In the tropics, the largest seasonal changes in the precipitation response appear to be a tendency towards a north-south split in the anomalies in the eastern Pacific during MAM, and strong east-west asymmetries in the anomalies during DJF with the anomalies of like sign in the Indian Ocean and western Pacific, and anomalies of opposite sign in between. The height field anomalies show a pronounced middle latitude response in the North Pacific/North American region during DJF, while JJA shows a weaker and more zonally-symmetric response. Schubert et al. (2002) found a similar tendency for zonal-symmetry in the boreal summer response to SST anomalies that occur on interannual time scales. In general, MAM tends to be more like DJF, while SON tends to have many of the characteristics of JJA. The cold seasons of the Northern Hemisphere tend to show substantial nonlinearities in the extratropical response (especially compare left and right top panels of Figs 7 and 8).

During the positive (wet) phase of the SST forcing (left panels of Figs. 7-8), the USGP precipitation anomalies are largely confined to the spring and summer seasons. The spring anomalies over the USGP appear to be associated with a negative height anomaly over the southwestern United States. During the summer the USGP precipitation anomalies appear to persist and/or develop somewhat further to the north of an anomalous ridge that develops over the south central United States. During the negative (dry) phase of the SST forcing (right panels of Figs 7-8), the USGP precipitation anomalies extend from the spring season well into the fall season. The longer-lived USGP

precipitation anomalies during the negative phase appear to be the result of the summer-like zonally-symmetric height response (with positive height anomalies over the United States) that lasts into the fall season. This is in contrast to the positive phase of the SST forcing under which the fall season (SON) shows a substantial seasonal change to an extratropical wave response over the United States that apparently counteracts the warm season wet conditions (lower left panel of Fig. 8).

To help assess the relative roles of the tropical and extratropical SST anomalies in the above idealized SST runs, we have carried out further experiments in which the EOF SST forcing is confined to the tropics (within +/- 20° latitude). The results of those experiments are very similar to those shown in the bottom panels of Figures 5 and 6, implying that the tropical SST dominate the response. In Fig. 9 we highlight the impact of the tropical SST on the USGP, by showing the temporal evolution of the precipitation in the USGP for the runs with the full (top panel) and tropical (bottom panel) EOF SST forcing. The three curves are for the positive SST EOF, negative SST EOF, and climate SSTs runs. Note that the tropical SST runs were only carried out for 30 years. The results show clearly that the positive (warm) phase produces a tendency for wet conditions while the cold phase produces dry conditions. The case with climatological SST tends to fall in between, although it is interesting to note that the run with climatological SST exhibits substantial variability such that at times it is as wet as the warm case (e.g. first 8 years and last 10 years), while at other times it is as dry as the cold case. We will return to an investigation of the climatological run in the next section. The bottom panel of Figure 9 shows that the tropical SST results are very similar to those with the full EOF forcing indicating that the main impact on the USGP precipitation comes from the tropical SST anomalies. The straight lines in Fig. 9 denote the time mean values of the USGP precipitation for the positive SST EOF, negative SST EOF, and climate SST runs. The mean values are all significantly different from each other (positive minus negative SST, positive minus climate SST, and negative minus climate SST) at the 5% level based on a t-test and assuming the anomalies are independent from one year to the next. If we assume instead that, only every other year is independent, then only the positive-negative SST and negative-neutral SST results are significant for

the global SST experiments, while only the positive-negative SST results are significant for the tropical SST experiment.

## 5. Land-Atmosphere Feedbacks

It is apparent from the top panel of Fig. 9 that the USGP precipitation exhibits long-term (decadal) fluctuations even in the absence of SST anomalies. In this section, we examine the nature of such fluctuations with a particular focus on the role of soil moisture feedbacks. We begin in section (i) by showing the various terms contributing to the soil moisture budget. In section (ii) we examine further the impact of soil moisture by making another 100-year simulation in which all feedbacks between the atmosphere and the soil wetness are turned off.

a) With land-atmosphere feedbacks

The top panel of Fig. 10 shows the time history of the annual mean precipitation, evaporation, and deep soil wetness (wet3) in the run with climatological SST (referred to hereafter as the control run). All three quantities exhibit long-term fluctuations. The precipitation fluctuations are similar in magnitude to those from the 70-year runs shown in Figure 1, even though those runs included observed SST variations. The bottom panel of Figure 10 shows the precipitation minus evaporation (P-E), and the net forcing on the soil moisture, namely the precipitation minus evaporation minus run-off (P-E-R). While P-E does show some low frequency variations, P-E-R looks to be largely a white noise process. We examine the lag correlations of these quantities in the next section. Note that P-E-R has a small negative bias. This imbalance in the moisture budget is the result of including lakes in the calculation of the area mean evaporation: these have, in the model formulation, an unlimited moisture supply.

Fig. 11 shows the correlations between the annual mean USGP precipitation and the global distribution of the 200mb heights (top panel) and the precipitation fields (bottom panel). In contrast to the results for the runs with SST anomalies, the correlations in this case show a more local wave train in the 200mb heights and precipitation (cf. Fig. 2) that extends from Alaska southeastward across North America and into the Atlantic. Separate calculations for DJF and JJA (not shown) indicate that the wave train occurs primarily during boreal winter, while during boreal summer the correlation with height and precipitation is very localized. One surprising aspect of the top panel of Fig. 11 is that there are substantial regions of negative correlations with the heights well away from the local response, over much of the tropical Indian Ocean and Indonesia, though these are only marginally significant (absolute values must exceed one-fifth to be significant at the 5% level using the Fisher's Z-transform and assuming 100 degrees of freedom). The nature of any connection to the tropical Indian Ocean/Indonesian region is unclear: note that there appears to be no signature of such a connection in the precipitation (bottom panel of Fig. 11).

b) Without land-atmosphere feedback

In order to examine the role of soil moisture variations in producing the long-term variations in precipitation shown in Figure 10, we have carried out a further 100-year simulation in which the effect of the soil moisture feedback is turned off. We do this by fixing the "$\beta$" (ratio of the evaporation to the potential evaporation) in the land surface model formulation to its seasonal climatology, as described in Koster et al. (2000). The specified values are interpolated between climatological monthly mean $\beta$s obtained from a 10-year segment of the simulation forced with climatological SST. Figure 12 (top panel) shows that the evaporation and more importantly the precipitation variations over the USGP are considerably reduced compared with the control run (cf. Figure 10). In fact, the precipitation variance is reduced by a factor of six, and the evaporation variance is reduced by a factor of 23 compared with the control run (both ratios are significant at the 5% level based on an F-test and assuming only 20 degrees of freedom in the 100 year run). The reduction in variance is qualitatively consistent with the results of Koster et al.

(2000). The middle and bottom panels of Fig. 12 show the precipitation in the USGP normalized to have zero mean and unit variance, for the fixed beta and control runs, respectively. These normalized results show more clearly that, in addition to impacting the amplitude of the rainfall variations, the interaction with soil moisture appears to also introduce longer time scales into the precipitation variations. Note for example, the 12-year period (years 61-72) of the control run with consistently negative precipitation (as well as deep soil wetness) anomalies. Also, the extended period of positive precipitation anomalies during years 30-40 is associated with an 11-year run of positive deep soil moisture anomalies. The probability of such strings of positive or negative values would be rather small if the year-to-year fluctuations in soil moisture were independent. For example, the probability of 11 consecutive negative values occurring (assuming equal probability of a positive or negative value) is $(1/2)^{11}$, or an average occurrence of roughly once every 2000 years.

The lag autocorrelation of the various terms in the moisture budget are shown in Table 2. For these

| | **Climate Run** | **Fixed β Run** |
|---|---|---|
| **Precipitation (P)** | **0.29** | 0.04 |
| **Evaporation (E)** | **0.37** | 0.03 |
| **Run-off (R)** | **0.20** | ----- |
| **Wet 2** | **0.39** | ----- |
| **Wet 3** | **0.48** | ----- |
| **P-E-R** | -.11 | ----- |

Table 2: Lag 1 autocorrelations of annual averages where the annual mean is computed over a water year (1 October – 30 September). Values in bold type are significant at the 5% level (see text).

statistics we have recomputed the annual averages to conform to a "water year" that begins 1 October. This is done to avoid introducing 1-year lag correlations that would occur due to spring melting of fall snow. To assess the statistical significance of the lag correlations, we generated 1000 cases of 100 independent realizations of a normal random variable with zero mean and unit variance. Each case was treated as a time series of 100 realizations and lag correlations were computed in the same way as for the model output. The 1000 values were then ordered from smallest to largest and the $50^{th}$ (-.17) and $950^{th}$ (+.15) values were taken as the lower and upper 5% significance levels.

The lag-autocorrelations for the fixed $\beta$ run are all insignificant, indicating that the annual mean evaporation and precipitation variations are white noise processes. For the control run, most quantities (P, E, R, and soil wetness) show significant lag-1 autocorrelations but then drop off rapidly (not shown). The deep soil (wet3) shows the greatest year-to-year memory with a lag 1 autocorrelation of about 0.5, though this high value must reflect in part the strong month-to-month autocorrelation of soil moisture, especially during freezing months. We note that the lag 2 autocorrelation in wet3 would be unaffected by any such month-to-month autocorrelation, and in fact the value (0.23) is consistent with a first order-autoregressive process where the autocorrelation decays as $0.5^k$, where k is the lag in years (see e.g. Box and Jenkins, 1976). The lag 3 autocorrelation (0.17) is marginally significant. As indicated earlier, the lag 1 autocorrelation in P-E-R (the net forcing on the soil) is not significant. We have also recomputed the correlations shown in Fig. 11 for the fixed $\beta$ run. The results (not shown) are generally quite similar to those in Fig. 11, though most of the remote correlations between the USGP and the heights (e.g. over the Indian Ocean) are absent.

The above results suggest that the low frequency (year-to-year memory) of the precipitation is tied to the long-term memory inherent in the deep soil. This is distinctly different from the month-to-month memory in the precipitation (e.g. Koster et al 2000) that is most affected by the faster time scales of atmospheric variability and the top layers of the soil. The low frequency soil moisture variations appear to be the result of the deep soil integrating the statistically white (on interannual time scales) noise forcing (P-E-R), in a process that is consistent with a red noise process. In fact, as

mentioned above, a candidate model for the soil moisture variations might be a first order autoregressive model, though the development and validation of such a model would likely require considerably longer integrations and is beyond the scope of the current analysis.

## 6. Discussion and Conclusions

The results of this study show that the NSIPP-1 model, when forced by observed SSTs, does produce low-frequency (multi-year) variations in the USGP precipitation similar to those observed. In particular, the model produces the dry conditions of the 1930s "dust-bowl" era. On the other hand, the model does not show a strong tendency for the dry conditions that were observed during the early 1950s (only one of the nine ensemble members reproduced the dry conditions). A correlative analysis suggests that the low frequency variations (time scales longer than about 6 years) in the USGP precipitation are linked to variations in a pan-Pacific decadal SST pattern, that is similar to patterns found in previous observation studies. This connection was confirmed by further AGCM simulations, in which the model was forced by the 2 polarities of the Pacific SST pattern. The idealized SST simulations further show that it is primarily that tropical part of the SST anomalies that influences the USGP. As such, the USGP tends to have above normal precipitation when the tropical Pacific SSTs are above normal, while there is a tendency for drought when the tropical SSTs are cold. The upper tropospheric response to pan-Pacific SST pattern shows a well-defined global-scale pattern with a strong wave response emanating from the tropical Pacific Ocean, and a substantial zonally-symmetric component in which USGP pluvial (drought) conditions are associated with reduced (enhanced) heights throughout the extra-tropics.

While there is a clear link between the USGP precipitation and the pan-Pacific SST pattern of variability, the SST account for only about 1/3 of the total low frequency variability in the precipitation. The remaining 2/3 of the variability in the low frequency USGP precipitation variability is internally generated. Results from a series of runs with climatological SSTs suggest

that the low frequency variations that occur in the absence of SST forcing require soil moisture feedback. In particular, simulations without soil moisture feedback show a six-fold decrease in the variance in annual USGP precipitation compared with simulations that include soil feedback. The interactions with the soil also introduce year-to-year memory in the hydrological cycle that is consistent with a red noise process, in which the low frequencies in the deep soil are the result of integrating a net forcing (precipitation – evaporation – runoff) that is white noise on interannual time scales. As such, the role of low frequency SST variability is to introduce a bias to the net forcing on the soil moisture that drives the random process preferentially to either wet or dry conditions.

There are a number of issues that require further analysis. The mechanism by which the SST impact the USGP precipitation is not clear. For example, the SST force a global scale response in the height field that is generally consistent with the precipitation changes over the USGP (reduced heights during pluvial conditions and enhanced heights during drought conditions), though exactly how that impacts the precipitation (in terms of changes in the storm tracks, suppressed rising motion, and changes in moisture transport) has not yet been established. We note that the zonally-symmetric component of the response on these long time scales is similar to the structure of the height response to tropical SST anomalies found on interannual time scales for boreal summer (Schubert et al. 2002).

A related issue concerns the link between the effects of ENSO and the effects of the low frequency pan Pacific SST mode on the USGP precipitation. It is not clear, for example, why the model generates consistently dry conditions during the 1930s, but not during the 1950s when the pan Pacific SST pattern has a sign and amplitude that is similar to that of the 1930s. In fact, the amplitude of the pan Pacific pattern is not particularly large during the 1930s. One reason for the difference could be the differences in the character of ENSO. The 1930s were characterized by a distinct lack of ENSO activity, suggesting it is the combination of weak ENSO and negative values of the pan Pacific SST pattern that is particularly conducive to drought in the USGP. As

such, we might consider ENSO warm events to periodically recharge the soil water reservoir, to help avoid prolonged (multi-year) drought conditions.

There are a number of issues that will require longer model simulations than the order 100-year simulations carried out here. For example, it would be desirable to have much longer idealized simulations in order to obtain more confidence in the lag-correlation statistics of the (decadal-scale) deep soil moisture fluctuations, including possible links to SST anomalies. There is, for example, some evidence for greater soil wetness/precipitation variability for the run with climate SST forcing, compared with either the warm or cold SST EOF forcing (see Fig. 9).

Finally, these results are clearly model dependent. The land surface model in the NSIPP model tends to have a stronger land-atmosphere coupling than other models (Koster et al. 2002). Assessing the model dependency will require comparisons with the results of other long simulations with several different models. Such runs are currently being carried out as part of the Climate of the 20$^{th}$ Century Project (WMO, 2001).

*Acknowledgements*: This work was supported by the NASA Earth Science Enterprise's Global Modeling and Analysis Program, and the NASA Seasonal-to-Interannual Prediction Project.

## References


Atlas, R., N. Wolfson and J. Terry, 1993: The effect of SST and soil moisture anomalies on the GLA model simulations of the 1988 U.S. drought. J. Climate, 6, 2034-2048.

Bacmeister, J., P.J. Pegion, S. D. Schubert, and M.J. Suarez, 2000: An atlas of seasonal means simulated by the NSIPP 1 atmospheric GCM, NASA Tech. Memo. No. 104606, volume 17, Goddard Space Flight Center, Greenbelt, MD 20771, 2000.

Bark, D.L., 1978: History of American Droughts. *North American Droughts.* AAAA Selected Symposia Series. Westview Press, Boulder Colorado, N.J. Rosenberg, Ed., pp 9-23.

Barlow, M., S. Nigam, and E.H. Berbery, 2000: ENSO, Pacific Decadal Variability, and U.S. summertime precipitation, drought, and streamflow. J. Climate

Barnett, T.P., L. Bengtsson, K. Arpe, M. Flugel, N. Graham, M. Latif, J. Ritchie, E. Roecker, U. Schlese, U. Schultzweida, and M. Tyree, 1994: Forecasting global ENSO-related climate anomalies. Tellus, 46A, 381-397.

Beljaars, A.C.M., P. Viterbo, M.J. Miller, and A.K. Betts, 1996: The anomalous rainfall over the United States during July 1993: Sensitivity to land surface parameterization and soil moisture anomalies, Mon. Wea. Rev., 124,362-383.

Borchert, J.R., 1971: The dust bowl in the 1970's. Assoc.Amer.Geogr.Ann., 61, 1-22.

Box, G.E.P and G.M. Jenkins, 1976: Time Series Analysis: Forecasting and Control, Holden Day, pp575.

Cayan,D., M. Dettinger, H. Diaz, and N. Graham, 1998: Decadal variability of precipitation over western North America. J. Climate, 11, 3148-3166.

Chou, M.-D., and M. J. Suarez, 1994: An efficient thermal infrared radiation parameterization for use in general circulation models. NASA Tech. Memo. 104606, Vol. 3, NASA Goddard Space Flight Center, Greenbelt, MD 20771, pp85.

Chou, M.-D. and M. J. Suarez, 1999: A solar radiation parameterization for atmospheric studies, NASA Technical Memorandum, 104606, vol. 11, NASA Goddard Space Flight Center, Greenbelt, MD 20771, 40pp.

Diaz,H., 1983: Drought in the United States – some aspects of major dry and wet periods in the contiguous United States, 1985-1981. J.Clim.Appl.Meteor., 22, 3-16.

Draper, N.R., and H. Smith, 1966: Applied Regression Analysis. John Wiley and Sons, Inc. pp407.

Erickson, C. O., 1983: Hemispheric anomalies of 700mb height and sea level pressure related to mean summer temperature over the United States. Mon. Wea. Rev., 111, 545-561.

Felch, R.E., 1978: Drought: Characteristics and assessment. *North American Droughts*. AAAA Selected Symposia Series. Westview Press, Boulder Colorado, N.J. Rosenberg, Ed., pp 25-42.

Helfand and S. D. Schubert, 1995: Climatology of the Simulated Great Plains Low-Level Jet and its Contribution to the Continental Moisture Budget of the United States. J. Climate, 8, 784-806.

Higgins, R., Y.Chen, A. Douglas, 1999: Interannual variability of the North American warm season precipitation regime. J.Climate, 12, 653-680.

Hughes, P., 1976: Drought: The land killer. American Weather Stories, U.S. Dept. Commerce, NOAA-EDS, Washington, D.C., pp77-87.

Kalnay, E., and Coauthors, 1996: The NCEP/NCAR 40-year reanalysis project. Bull. Amer.Meteor.Soc., 77, 437-471.

Karl,T., and A. Koscielny, 1982: Drought in the United States: 1895-1981. J. Climatolog., 2, 313-329.

Koster, R.D. and M.J. Suarez, 1996: Energy and water balance calculations in the Mosaic LSM, NASA Tech. Memo. 104606, vol. 9, pp194.

Koster R.D., M.J. Suarez, M. Heiser, 2000: Variance and predictability of precipitation at seasonal-to-interannual timescales. J. Hydrometeor., 1, 26-46.

Koster R.D., P.A. Dirmeyer, A.N. Hahmann, R.Ijpelaar, L. Tyahla, P. Cox, and M.J. Suarez, 2002: Comparing the degree of land-atmosphere interaction in four atmospheric general circulation models. J. Hydrometeor., 3, 363-375.

Livezey, R. and T.Smith, 1999: Covariability of aspects of North American climate with global sea surface temperatures on interannual to interdecadal timescales. J.Climate, 12, 289-302.

Louis, J., M. Tiedtke, J. Geleyn, 1982: A short history of the PBL parameterization at ECMWF, in *Proceedings, ECMWF Workshop on Planetary Boundary Layer Parameterization*, Reading, U. K., 59-80.

Lyon, B. and R.M. Dole, 1995: A diagnostic comparison of the 1980 and 1988 U.S. summer heat wave-droughts. J. Climate, 8, 1658-1676.

Mantua, N., S. Hare, Y. Zhang, J.M. Wallace, and R. Francis, 1997: A Pacific interdecadal climate oscillation with impacts on salmon production. Bull.Amer.Meteor.Soc., 78, 1069-1079.

Mo, K.C., J. Nogues-Paegle, and R.W. Higgins, 1997: Atmospheric processes associated with summer floods and droughts in the central United States. J.Climate Sci., 10, 3028-3046.

Montroy,D., 1997: Linera relation of central and eastern North American precipitation to tropical Pacific sea surface temperature anomalies. J.Climate, 10, 541-558.

Moorthi, S. and M. J. Suarez, 1992: Relaxed Arakawa-Schubert: A parameterization of moist convection for general circulation models. *Mon. Wea. Rev.*, 120, 978-1002.

Namias, J., 1955: Some meteorological aspects of drought with special reference to the summers of 1952-1954 over the United States. Mon.Wea.Rev., 83, 199-205.

Namias, J., 1982: Anatomy of Great Plains protracted heat waves (especially the 9180 U.S. summer drought). Mon.Wea.Rev., 110,824-838.

Pegion, P.J., S. D. Schubert, and M.J. Suarez, 2000: An assessment of the predictability of northern winter seasonal means with the NSIPP 1 AGCM, NASA Tech. Memo. No. 104606, volume 18, Goddard Space Flight Center, Greenbelt, MD 20771, 2000.

Rayner, N.A., Horton, E.B., Parker, D.E., Folland, C.K., and Hackett, R.B., 1996: Version 2.2 of the global sea-ice and sea surface temperature data set, 1903-1994. Climate Research Technical Note No. 74, The Met Office.

Rayner, N.A., Parker, D.E., Horton, E.B., Folland, C.K., Alexander, L.V. and Rowell, D.P., 2002: Globally complete analyses of SST, sea ice and night marine air temperature, 1871-2000. *J. Geophys. Res. (Oceans)*, in preparation.

Reynolds, W. R. and T. M. Smith, 1994: Improved global sea surface temperature analyses using optimum interpolation. J. Climate, 7, 929 -948.

Ropelewski, C. and M. Halpert, 1986: North American precipitation and temperature patterns associated with El Nino/Southern Oscillation (ENSO). Mon.Wea.Rev., 114, 2352-2362.

Rosenberg, N.J., 1978: North American Droughts. AAAA Selected Symposia Series. Westview Press, Boulder Colorado, N.J. Rosenberg, Ed., 177pp.

Rowell, D. P., C. Folland, K. Maskell, and N. Ward, 1995: Variability of summer rainfall over tropical north Africa (1906-92): Observations and modeling. Q.J.R.Meteor.Soc., 121, 669-704.

Schubert,S.D., M.J. Suarez, P.J. Pegion, M.A. Kistler, and A. Kumer, 2002: Predictability of zonal means during boreal summer,", J.Climate, 15, 420-434.

Stuart, A. and J.K. Ord, 1994: Kendall's Advanced Theory of Statistics. Halsted Press, New York, 676pp.

Suarez, M. J. and L. L. Takacs, 1995: *Documentation of the Aries-GEOS Dynamical Core:Version 2.* NASA Tech. Memo. No. 104606, volume 5, Goddard Space Flight Center, Greenbelt, MD 20771.

Ting, M., 1994: Maintenance of northern summer stationary waves in a GCM. J. Atmos. Sci., 51,3286-3308.

Ting, M. and H. Wang, 1997: Summertime U.S. precipitation variability and its relation to Pacific Sea Surface Temperature, J. Climate, 10,1853-1873.

Trenberth, K.E., G.W. Branstator and P.A. Arkin, 1988: Origins of the 1988 North American drought. Science, 242, 1640-1645.

Trenberth, K., 1990: Recent observed interdecadal climate changes in the Northern Hemisphere. Bull. Amer.Meteor.Soc., 71, 988-993.

Trenberth, K.E. and G.W. Branstator, 1992: Issues in establishing causes of the 1988 drought over North America. J. Climate, 5, 159-172.

Van den Dool, H. M., J. Hoopingarner, E.O'Lenic, A.J.Wagner, A.G.Barnston, R.E.Livezey, D.Unger, A.Artusa and R.Churchill, 1999: Third Annual review of skill of CPC real time long lead predictions: How well did we do during the great ENSO event. Proceedings of the 23rd Annual Climate Diagnostics and Prediction Workshop, Oct. 26-30, 1998, Miami, Florida. U.S. Department of Commerce, NOAA/NWS/NCEP/CPC 336pp.

Von Storch, H. and F.W. Zwiers, 1999: Statistical analysis in climate research. Cambrideg University Press, 484pp.

Vose,R., R. Schmoyer, P. Steurer, T. Peterson, R. Heim, T. Karl, and J. Eischeid, 1992: *The Global Historical Climatology Network: long-term monthly temperature, precipitation, sea level pressure, and station pressure data.* ORNL/CDIAC-53, NDP-041. Carbon Dioxide Information Analysis Center, Oak Ridge National Laboratory, Oak Ridge, Tennessee.

Wallace, J. M., and D. S. Gutzler, 1981: Teleconnections in the geopotential height field during the Northern Hemisphere winter. Mon. Wea. Rev., 109, 784-812.

WMO, 2001: Report of the sixteenth session of the CAS/JSC Working Group on Numerical Experimentation. *WMO TD 1076*

Woodhouse, C.A. and J.T. Overpeck 1998: 2000 years of drought variability in the central United States. Bull.Amer.Meteor.Soc., 79, 2693-2714.

Worster, D., 1979: Dust Bowl: The Southern Great Plains in the 1930s. Oxford University Press, New York, 277pp.

Xie, P. and P. Arkin, 1996: Analyses of global monthly precipitation using gauge observations, satellite estimates and numerical model predictions. J. Climate, 9, 840-858.

Zhang, Y., J.M. Wallace, and D. Battisti, 1997: ENSO-like interdecadal variability: 1900-93. J. Climate, 10, 1004-1020.

Zwiers, F.W., X.L. Wang and J. Sheng, 2000: Effects of specifying bottom boundary conditions in an ensemble of atmospheric GCM simulations. J. Geophys. Res., 105, 7295-7315.

**List of Figures**

Figure 1: Time series of precipitation anomalies averaged over the USGP (30°-50°N, 95°-105°W). A filter is applied to remove time scales shorter than about 6 years. The thin black curves are the results from the nine ensemble members produced with the NSIPP-1 model forced by observed SST. The thin curves are dashed for the time periods where the filter crosses discontinuities in the runs. The thick solid curve is the ensemble mean. The thick dashed curve is the observational estimate (see text). Units: mm/day.

Figure 2: The correlation between the filtered (time scales greater than 6 years) ensemble mean precipitation averaged over the USGP (30°-50°N, 95°-105°W) and SST (top panel), filtered ensemble mean precipitation (middle panel), and filtered ensemble mean 200mb height (bottom panel), for the period 1930-1999.

Figure 3: Top left panel: The leading EOF of the low-pass filtered (greater than 6 years) SST for the period 1930-1999. Top right panel: The leading EOF of the residual SST (unfiltered annual mean – low pass). Lower panel: The time series of the principal components (pcs) of the leading low pass (black curve) and residual (red curve) EOFs. Units of the pcs is standard deviations. The product of the pcs and the spatial maps gives units of °C. The SST EOFs are computed from HADISST data for the period 1930-1999.

Figure 4: Top panel: The correlation between the leading low frequency SST principal component (Fig. 3) and the ensemble mean low frequency precipitation for the period 1930-1999. Bottom panel: The correlation between the leading residual (total – low frequency) SST principal component (Fig. 3) and the ensemble mean residual precipitation for the period 1930-1999. The residuals have a 5-month running mean applied before computing the correlations.

Figure 5: Top left panel: Composite 200mb height anomaly, computed from the ensemble mean low pass filtered data. The composite includes all time periods in which the leading low pass SST EOF (see Figure 3) has PC values greater than 1 standard deviation. Values are scaled to be representative of 2 standard deviations. Top right panel: Same as top left panel, except for when the PC values are less than –1 standard deviations. Lower left panel: Annual mean 200mb height anomaly from the 40-year run forced with +2 standard deviations in the leading low pass filtered SST EOF. Lower right panel: Annual mean 200mb height anomaly from the 40-year run forced with -2 standard deviations in the leading low pass filtered SST EOF. In the right panels the sign is changed to help show any nonlinearities in the response. In the lower panels only, values are shaded only where they are significant at the 5% level based on a t-test. Units: meters.

Figure 6: Same as Figure 5, except for precipitation. Units: mm/day.

Figure 7: The seasonal cycle of the response to the idealized SST EOF forcing. The left panels are for the run with +2 standard deviations in the leading low pass filtered SST EOF. The right panels

are for the run with -2 standard deviations in the leading low pass filtered SST EOF. In the right panels the sign is changed to help show any nonlinearities in the response. Shading indicates those regions with differences significant at the 5% level based on a t-test.

Figure 8: Same as Figure 7, except for the 200 mb height field.

Figure 9: Top panel: Time series of the annual mean precipitation over the USGP (30°-50°N, 95°-105°W) from the runs forced with the leading low pass filtered SST EOF (Figure 5). The red curve is for the run forced with +2 standard deviations in the EOF. The blue curve is for the run forced with –2 standard deviations in the EOF. The black curve is the control run using climatological SSTs. The straight lines are the corresponding time means. The SST climatology and the EOFs used in the runs were computed from the HADISST data for the period 1930-1999. Bottom panel: Same as top panel, except that the SST anomalies are set to zero poleward of 20° latitude. Units: mm/day.

Figure 10: Top panel: Time series of the annual mean precipitation (green curve), evaporation (red curve) and wet3 (deep soil moisture, blue curve) over the USGP (30°-50°N, 95°-105°W), from the control run with climatological SSTs. The units for precipitation and evaporation are mm/day (left ordinate), and they are dimensionless (values range from 0-1) for wet3 (right ordinate).
Bottom panel: Same as the top panel, except for the time series of the annual mean precipitation minus evaporation (red curve) and precipitation minus evaporation minus run-off (blue curve). Units are mm/day.

Figure 11: The correlation between the annual mean precipitation anomalies over the USGP and 200mb height (top panel), and precipitation (bottom panel) for the 100-year control run with climatological SST. Correlations with absolute value greater than 1/5 are significant at the 5% level using the Fisher's Z-transform and assuming 100 degrees of freedom.

Figure 12: Same as top panel of Fig.10, except for the run with climatological SST and fixed $\beta$. The green curve is the precipitation and the red curve is the evaporation (red curve). Note that the soil moisture (wet3) plays no role in this run. The middle panel shows the precipitation from the fixed beta run standardized to have zero mean and unit variance. The bottom panel is the same as the middle panel except for the control run.

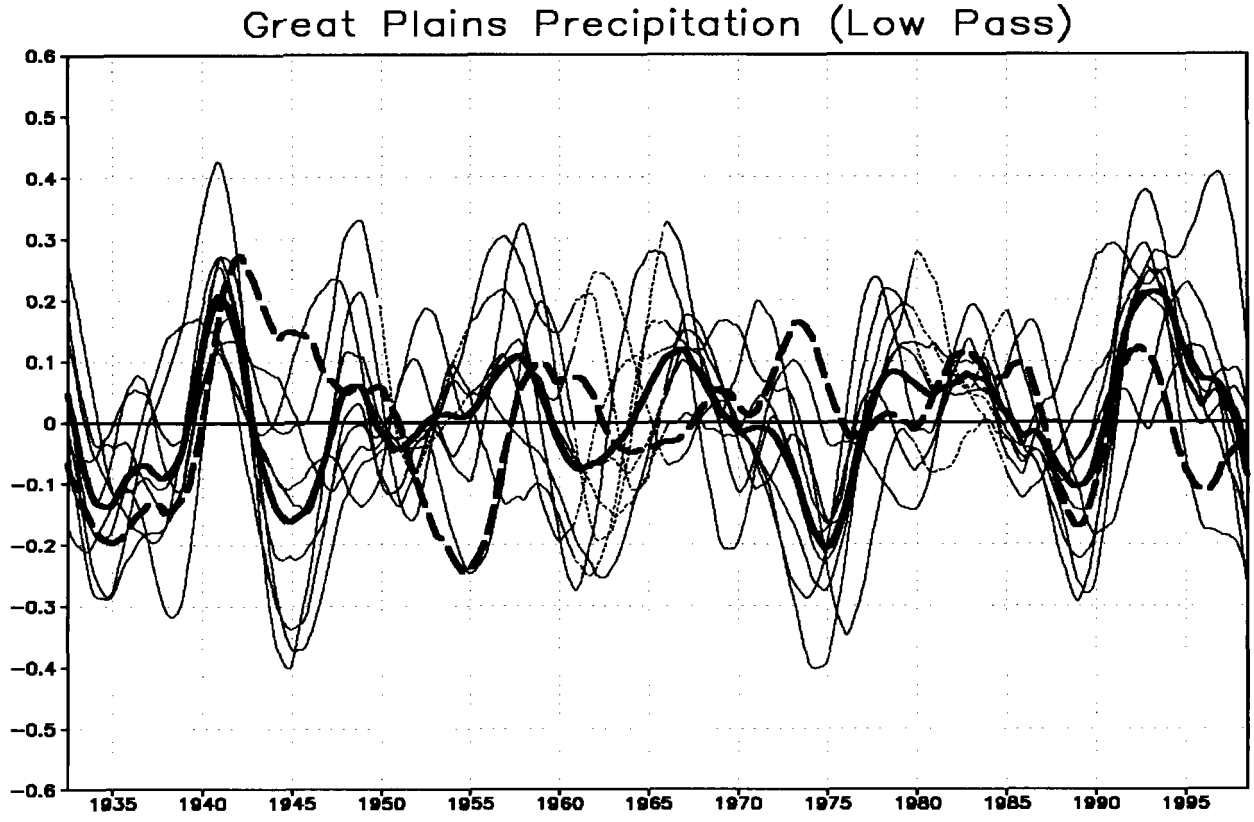


Figure 1: Time series of precipitation anomalies averaged over the USGP (30°-50°N, 95°-105°W). A filter is applied to remove time scales shorter than about 6 years. The thin black curves are the results from the nine ensemble members produced with the NSIPP-1 model forced by observed SST. The thin curves are dashed for the time periods where the filter crosses discontinuities in the runs. The thick solid curve is the ensemble mean. The thick dashed curve is the observational estimate (see text). Units: mm/day.

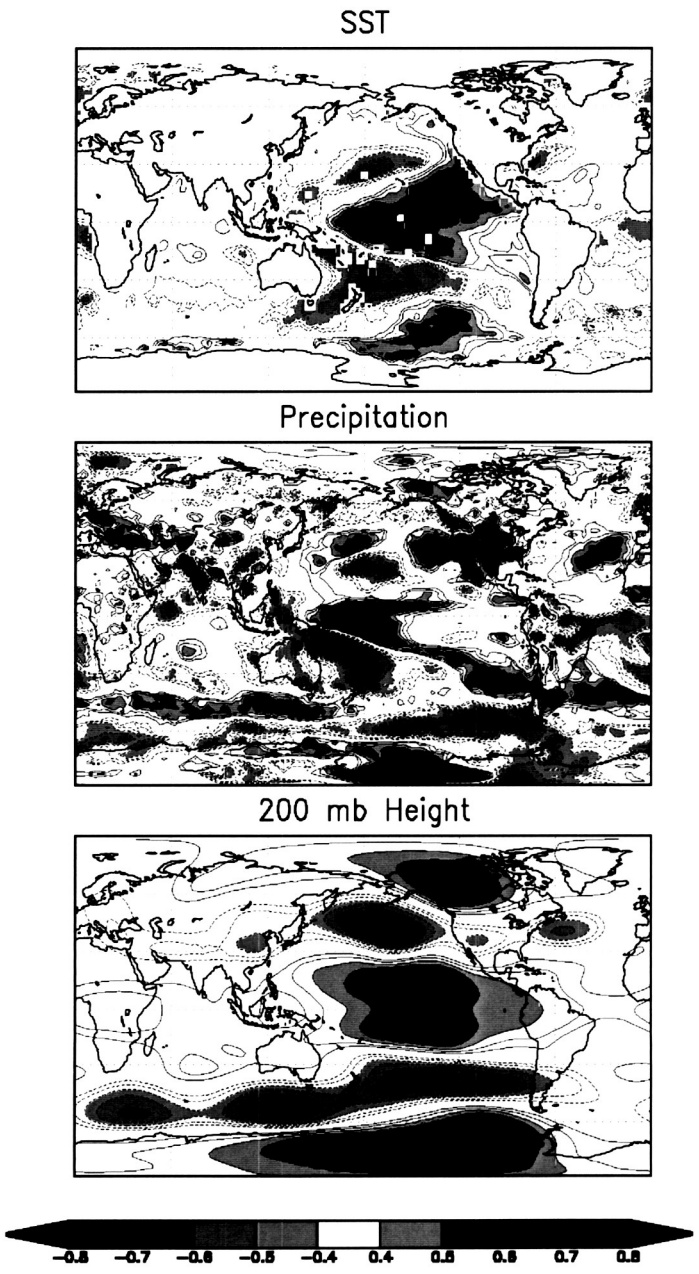


Figure 2: The correlation between the filtered (time scales greater than 6 years) ensemble mean precipitation averaged over the USGP (30°-50°N, 95°-105°W) and SST (top panel), filtered ensemble mean precipitation (middle panel), and filtered ensemble mean 200mb height (bottom panel), for the period 1930-1999.

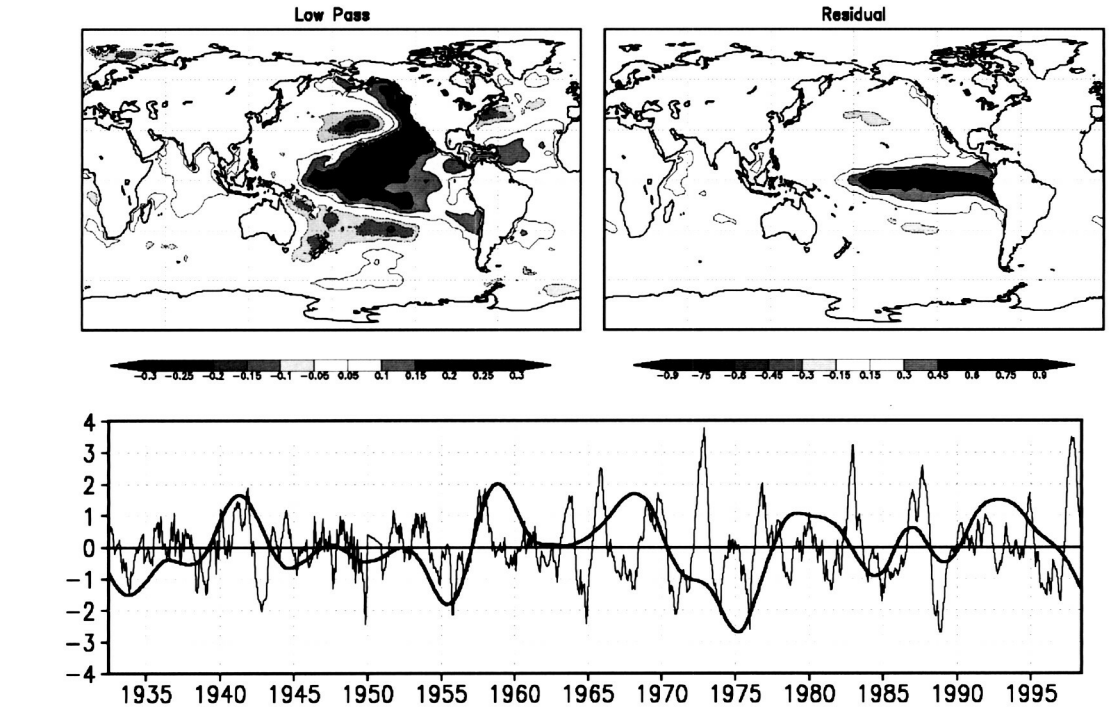


Figure 3: Top left panel: The leading EOF of the low-pass filtered (greater than 6 years) SST for the period 1930-1999. Top right panel: The leading EOF of the residual SST (unfiltered annual mean – low pass). Lower panel: The time series of the principal components (pcs) of the leading low pass (black curve) and residual (red curve) EOFs. Units of the pcs is standard deviations. The product of the pcs and the spatial maps gives units of °C. The SST EOFs are computed from HADISST data for the period 1930-1999.

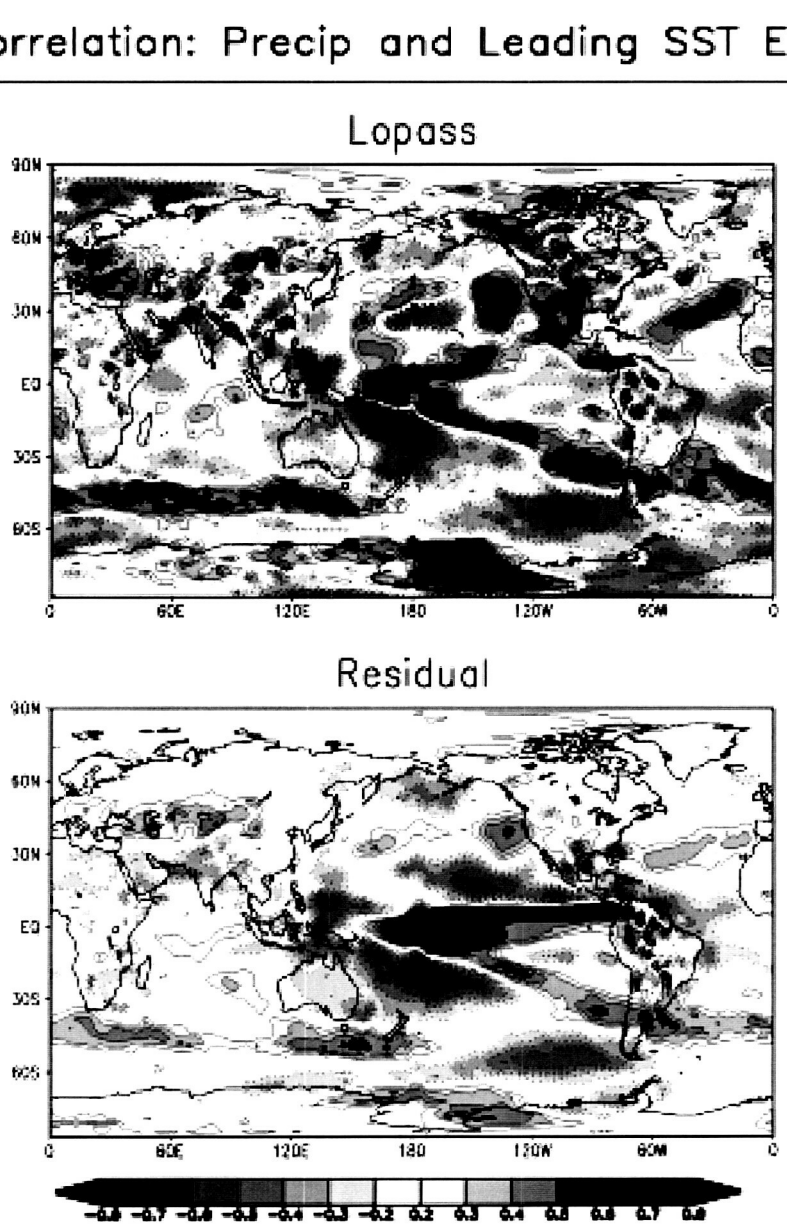


Figure 4: Top panel: The correlation between the leading low frequency SST principal component (Fig. 3) and the ensemble mean low frequency precipitation for the period 1930-1999. Bottom panel: The correlation between the leading residual (total – low frequency) SST principal component (Fig. 3) and the ensemble mean residual precipitation for the period 1930-1999. The residuals have a 5-month running mean applied before computing the correlations.

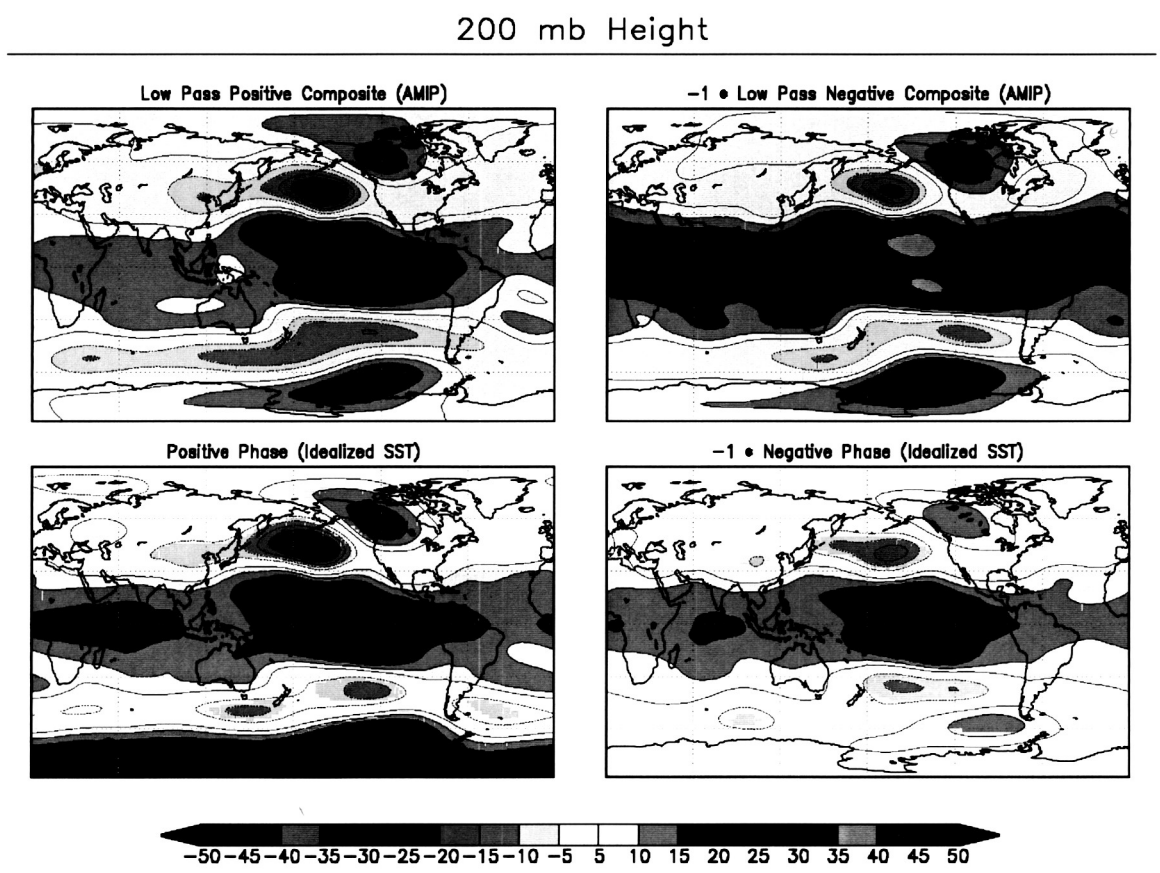


Figure 5: Top left panel: Composite 200mb height anomaly, computed from the ensemble mean low pass filtered data. The composite includes all time periods in which the leading low pass SST EOF (see Figure 3) has PC values greater than 1 standard deviation. Values are scaled to be representative of 2 standard deviations. Top right panel: Same as top left panel, except for when the PC values are less than –1 standard deviations. Lower left panel: Annual mean 200mb height anomaly from the 40-year run forced with +2 standard deviations in the leading low pass filtered SST EOF. Lower right panel: Annual mean 200mb height anomaly from the 40-year run forced with -2 standard deviations in the leading low pass filtered SST EOF. In the right panels the sign is changed to help show any nonlinearities in the response. In the lower panels only, values are shaded only where they are significant at the 5% level based on a t-test. Units: meters.

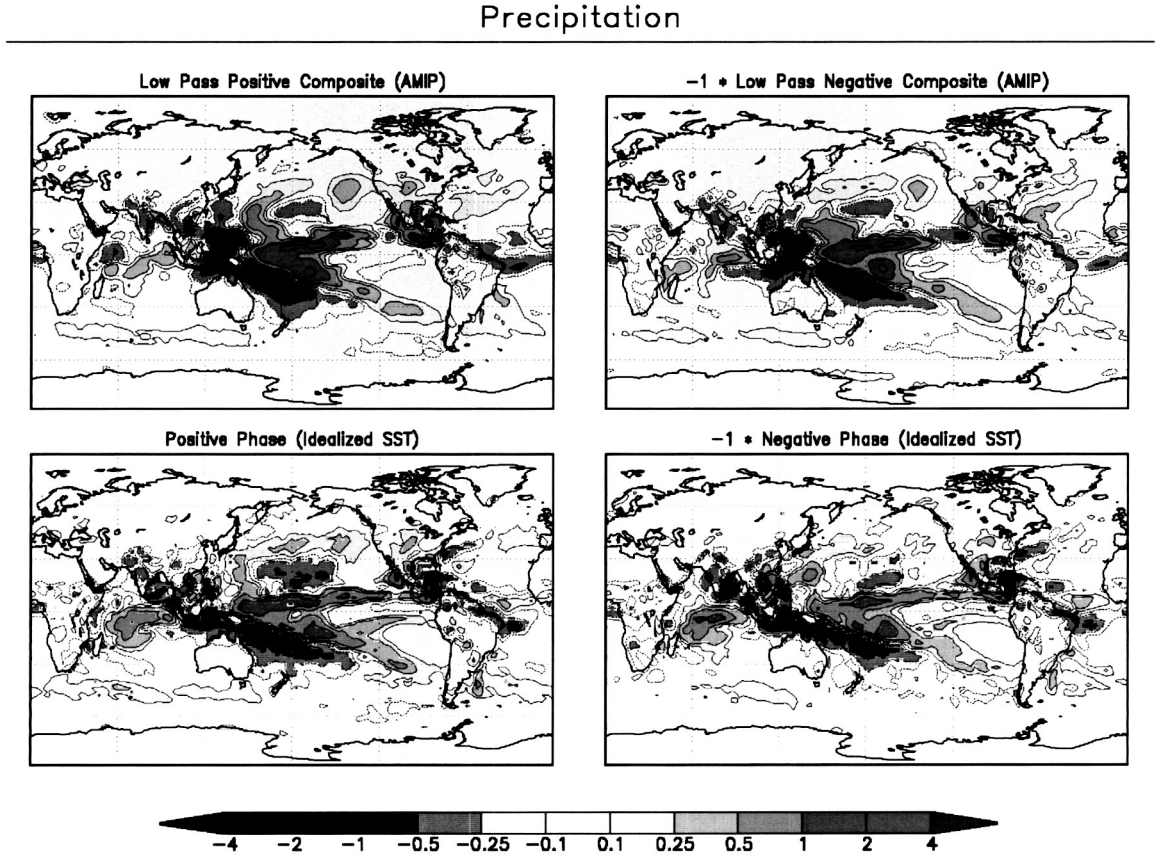


Figure 6: Same as Figure 5, except for precipitation. Units: mm/day.

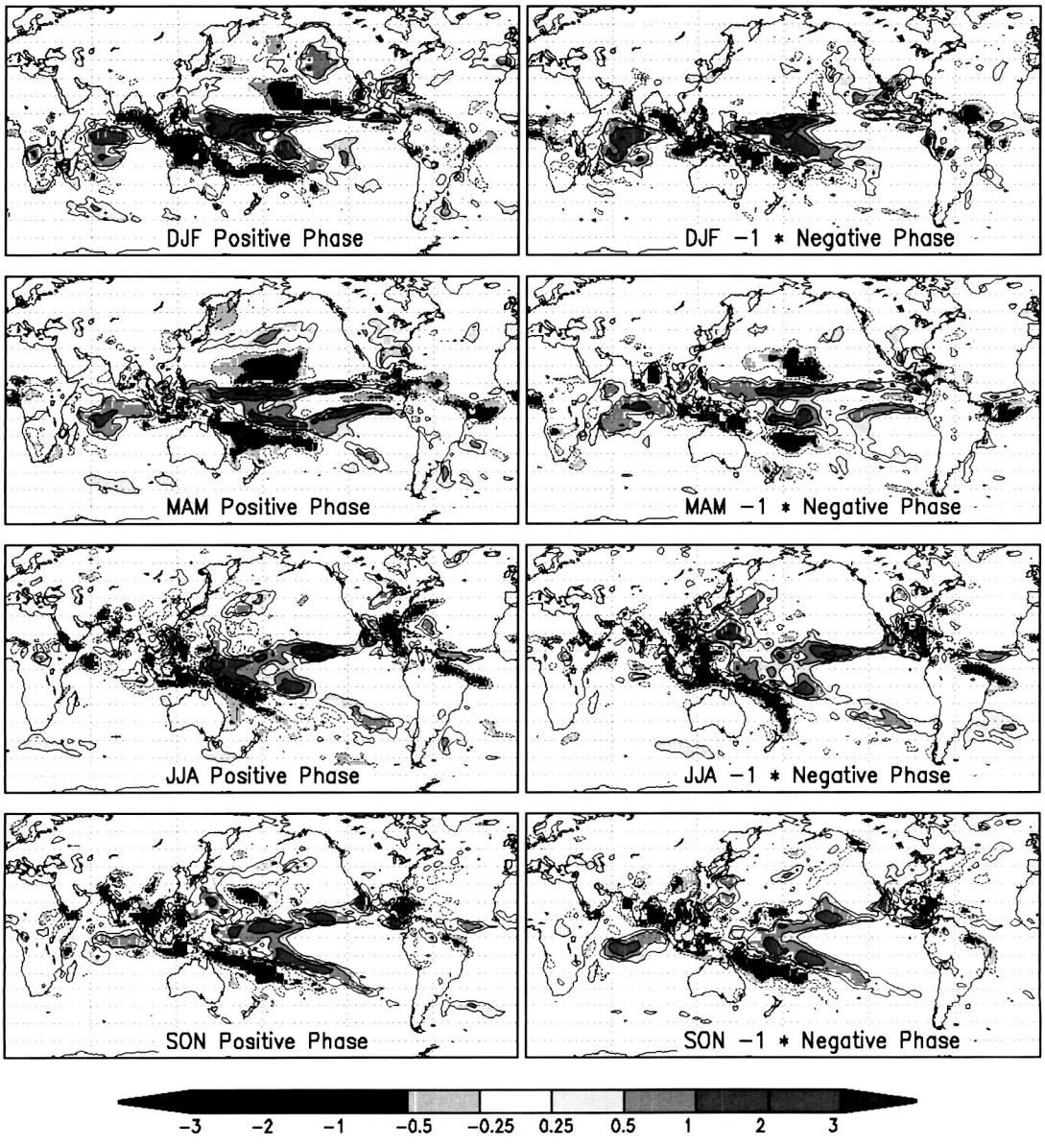


Figure 7: The seasonal cycle of the response to the idealized SST EOF forcing. The left panels are for the run with +2 standard deviations in the leading low pass filtered SST EOF. The right panels are for the run with -2 standard deviations in the leading low pass filtered SST EOF. In the right panels the sign is changed to help show any nonlinearities in the response. Shading indicates those regions with differences significant at the 5% level based on a t-test.

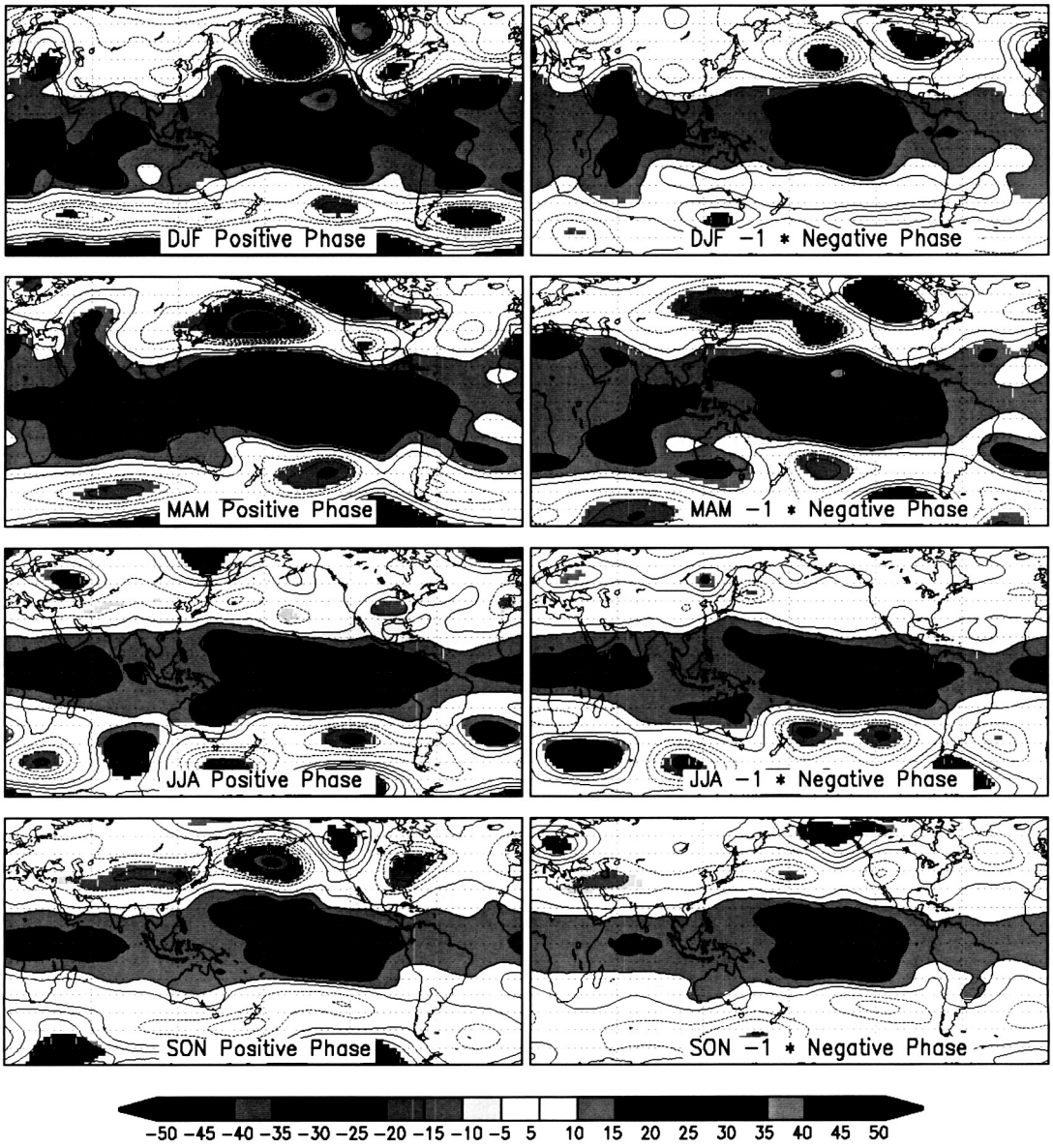


Figure 8: Same as Figure 7, except for the 200 mb height field.

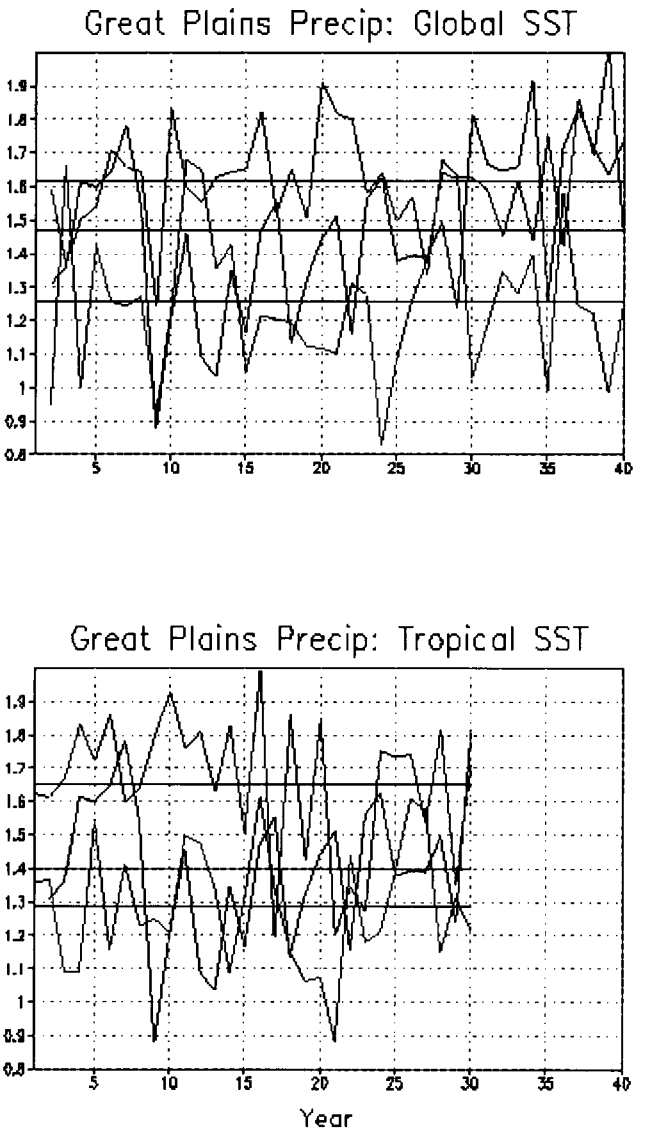


Figure 9: Top panel: Time series of the annual mean precipitation over the USGP (30°-50°N, 95°-105°W) from the runs forced with the leading low pass filtered SST EOF (Figure 5). The red curve is for the run forced with +2 standard deviations in the EOF. The blue curve is for the run forced with –2 standard deviations in the EOF. The black curve is the control run using climatological SSTs. The straight lines are the corresponding time means. The SST climatology and the EOFs used in the runs were computed from the HADISST data for the period 1930-1999. Bottom panel: Same as top panel, except that the SST anomalies are set to zero poleward of 20° latitude. Units: mm/day.

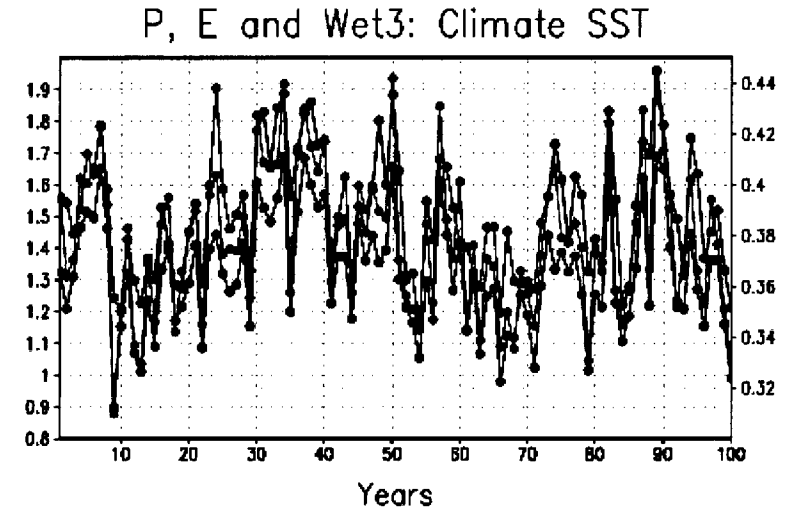


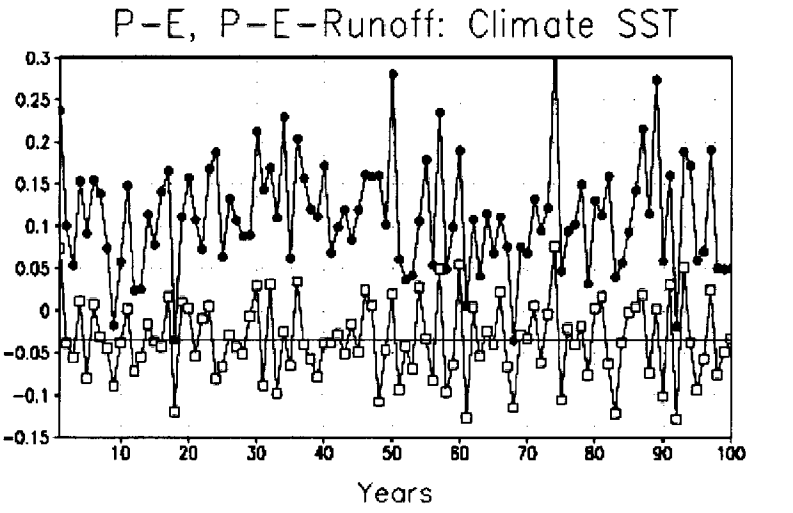


Figure 10: Top panel: Time series of the annual mean precipitation (green curve), evaporation (red curve) and wet3 (deep soil moisture, blue curve) over the USGP (30°-50°N, 95°-105°W), from the control run with climatological SSTs. The units for precipitation and evaporation are mm/day (left ordinate), and they are dimensionless (values range from 0-1) for wet3 (right ordinate).

Bottom panel: Same as the top panel, except for the time series of the annual mean precipitation minus evaporation (red curve) and precipitation minus evaporation minus run-off (blue curve). Units are mm/day.

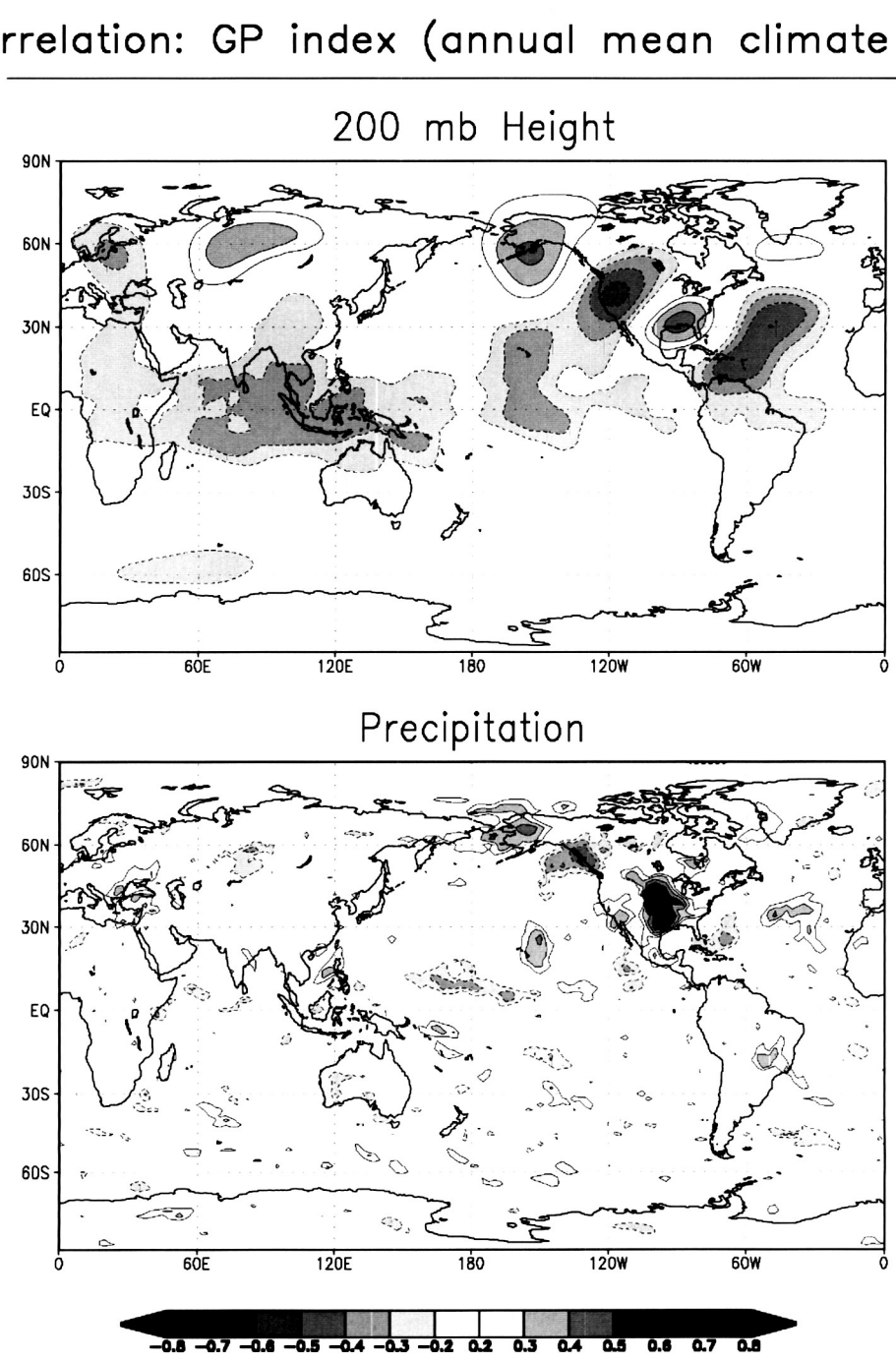


Figure 11: The correlation between the annual mean precipitation anomalies over the USGP and 200mb height (top panel), and precipitation (bottom panel) for the 100-year control run with climatological SST. Correlations with absolute value greater than 1/5 are significant at the 5% level using the Fisher's Z-transform and assuming 100 degrees of freedom.

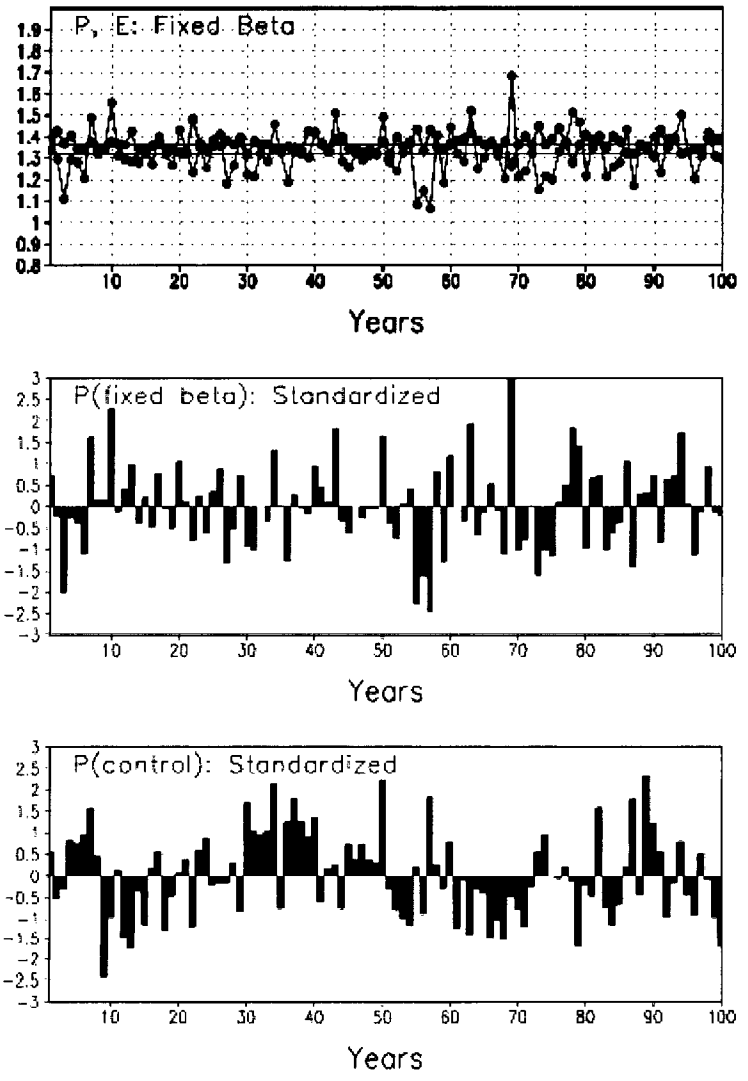


Figure 12: Same as top panel of Fig.10, except for the run with climatological SST and fixed β. The green curve is the precipitation and the red curve is the evaporation (red curve). Note that the soil moisture (wet3) plays no role in this run. The middle panel shows the precipitation from the fixed beta run standardized to have zero mean and unit variance. The bottom panel is the same as the middle panel except for the control run.

Popular summary of the manuscript "Causes of Long-Term Drought in the United States Great Plains" by Siegfried D. Schubert, Max J. Suarez, Philip J. Pegion[1], and Randal Koster

3 July 2002

(Paper submitted to J. Climate)

The United States Great Plains experienced a number of long-term droughts during the last century, most notably the droughts of the 1930s and 1950s. In this study, we examined the causes of such droughts using long-term (70-year, 1930-1999) simulations of the global atmosphere using an atmosphere/land general circulation model (AGCM) developed as part of the NASA Seasonal-to-Interannual Prediction Project. The AGCM is forced during the 70-year integration with the observed sea surface temperatures (SSTs), and our interest is in how the atmosphere and land respond to that forcing on long (multi-year) time scales. To do this we actually carry out several (nine) different 70-year simulations with exactly the same SST forcing but where each run starts out from slight different atmospheric/land initial conditions. From these runs, we are able to determine what part of the variations in, for example, precipitation, are forced by the SST (the average of the nine runs), and what part of the variations are not forced by the SST (the internally-generated variability determined from the deviations about the average of the nine runs).

The results of our model simulations suggest that the long-term variations in precipitation in the Great Plains are forced by a large-scale pattern of SST variability that spans much of the Pacific Ocean. We further show that it is primarily the tropical part of the Pacific SST that is important for the Great Plains. The impact of the SST on the rainfall in the Great Plains is, however, rather modest when compared with other internally generated and largely unpredictable rainfall variations that occur in that region. We go on to show that this internally-generated variability in the precipitation is due to interactions with soil moisture. Apparently, the interactions between the soil moisture and the atmosphere can lead to long-term drought in the Great Plains even in the absence of SST forcing.